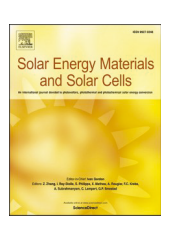
ELSEVIER

Contents lists available at ScienceDirect

Solar Energy Materials and Solar Cells

journal homepage: http://www.elsevier.com/locate/solmat





Stable magnesium zinc oxide by reactive Co-Sputtering for CdTe-based solar cells

Yegor Samoilenko ^a, Gavin Yeung ^a, Amit H. Munshi ^b, Ali Abbas ^c, Carey L. Reich ^b, Michael Walker ^e, Matthew O. Reese ^d, Andriy Zakutayev ^d, J. Michael Walls ^c, Walajabad S. Sampath ^b, Colin A. Wolden ^{a,e,*}

- ^a Department of Chemical and Biological Engineering, Colorado School of Mines, Golden, CO, 80401, USA
- b NGPV (Next Generation PV Center), Department of Mechanical Engineering, Colorado State University, Fort Collins, CO, 80523, USA
- c CREST, Wolfson School of Mechanical, Electrical and Manufacturing Engineering, Loughborough University, Loughborough, LE11 3TU, UK
- ^d Materials Science Center, National Renewable Energy Laboratory, Golden, CO, 80401, USA
- ^e Materials Science Program, Colorado School of Mines, Golden, CO, 80401, USA

ARTICLE INFO

Keywords: CdTe Thin film photovoltaics $Mg_xZn_{1-x}O$ Reactive sputtering Stability

ABSTRACT

Magnesium zinc oxide (MZO) is a promising front contact material for CdTe solar cells. Due to its higher band gap than traditional CdS, MZO can reduce parasitic absorption to significantly increase short-circuit current density while also providing a benefit of conduction band offset tuning through Mg:Zn ratio optimization. MZO has been successfully implemented into CdTe devices, however its stability has been of concern. The MZO stability issue has been attributed to the presence of oxygen in the CdTe device processing ambient, leading to double-diode behavior (S-kink) in the current density-voltage curves. Here we report on MZO thin films deposited by reactive co-sputtering. The reactively co-sputtered MZO thin films have encouraging stability, show no significant variation in work function of the surface over a period of 6 months, as measured by Kelvin probe. Energy conversion efficiencies of around 16% have been achieved both with and without presence of oxygen in device processing ambients across multiple research facilities. These efficiencies should be possible to increase further by tuning of the thin film deposition and device processing parameters, especially through optimization of the back contact.

1. Introduction

Cadmium telluride (CdTe) thin film photovoltaic technology has become a commercial leader with over 25 GW installed capacity worldwide [1]. In recent years, the efficiency has been improved significantly to reach 22.1% [2], primarily through alloying CdTe with Se and substitution of CdS as a window layer with wider band gap materials, both of which allow for improved short circuit current density (J_{sc}), such that they are close to theoretical limits in champion devices [3,4]. Nevertheless, further increases in efficiency can be achieved through improvements in open circuit voltage (V_{oc}) and fill factor (FF), which is still well below its theoretical maximum. A key to achieving these improvements is higher carrier concentration and lifetime [5,6]. Significant progress has been made in those areas through group V doping and Se alloying, respectively [7–9]. However, to fully realize these benefits improved emitter layers are required [5]. The ideal

emitter should be transparent, have appropriate conduction band position and doping levels, and it must be chemically compatible with both the materials and device processing [10-12].

Magnesium zinc oxide ($Mg_xZn_{1-x}O$, MZO) has been demonstrated to be a superior emitter to conventional CdS [10]. MZO is transparent (Eg >3.3 eV) and its conduction band edge can be appropriately aligned with the CdTe absorber by tuning the degree of Mg incorporation, reducing interface recombination. Optimal performance requires flat or slightly positive conduction band offset [10–12]. In addition, in double heterostructures it has been shown that MZO passivates CdTe and results in higher carrier lifetime [13]. Despite these successes, concerns remain about the stability of MZO [14], and its use constraints the conditions used for subsequent device processing. In particular, it imposes a requirement that no oxygen may be used in subsequent processing, as its presence has been attributed to formation of an "S-kink" in the current density-voltage (J-V) curves [15,16]. Another unresolved challenge has

^{*} Corresponding author. Department of Chemical and Biological Engineering, Colorado School of Mines, Golden, CO, 80401, USA. *E-mail address:* cwolden@mines.edu (C.A. Wolden).

been the achievement of stable doping levels in MZO.

To date the MZO films integrated into CdTe solar cells have been produced almost exclusively by sputtering using ceramic targets [3, 15–17]. This limits exploration of composition to discrete values, and the optimal Mg/Zn value remains unclear and is likely to be a function of both the specific device architecture and processing steps employed. In addition, ceramic targets are expensive, have relatively low deposition rates, and suffer from target aging and poor utilization, so metal targets are desirable for MZO sputtering [18]. There have been several reports on combinatorial deposition of MZO [19,20], including co-sputtering from Mg metal and ZnO ceramic targets [21], but without integration in CdTe photovoltaic devices.

Here, we demonstrated a combinatorial reactive co-sputtering of MZO films from Mg and Zn targets for application as emitters in CdTe photovoltaic solar cell devices. This deposition approach allows the composition and thickness of MZO film to be varied continuously on one substrate by keeping it stationary during deposition. These combinatorial MZO libraries are then converted into photovoltaic devices by depositing CdTe on top of them, accelerating optimization of solar cells. Optimization of device performance led to device efficiencies of around 16% with oxygen present in the device processing ambient. We hypothesize that native point defects are the origin of MZO instability in other studies, and that the concentration of these defects is stabilized by sputtering in an oxygen ambient in this report. The robust nature of reactively sputtered MZO was validated by its use for successful CdTe device fabrication across multiple laboratories.

2. Materials and Methods

MZO films were deposited by reactive co-sputtering from elemental Zn (99.99%) and Mg (99.95%) targets in an AJA Orion-5 chamber at a substrate to target distance of 10 cm. DC power supply was used for Zn sputtering, while RF was used for Mg. TEC10 glass (Hartford Glass) superstrates were used for devices and were cleaned prior to being loaded into the sputter chamber using Micro 90 solution followed by a 20-min UV-ozone treatment. Si wafers and glass slides were used for MZO thickness and band gap measurements, respectively, and were cleaned in isopropanol prior to being loaded into the sputter chamber. Plasma clean at 50 W for 5 min in 5 mTorr of Ar was performed on all substrates right before MZO deposition. The substrate was held stationary during deposition of combinatorial libraries; the substrate was rotated to produce single composition films. Typical thicknesses of MZO on a 3" combinatorial library ranged from 80 to 150 nm with deposition rates of about 0.67-1.25 nm/min at higher and lower band gaps, respectively. Argon and oxygen were supplied in a 2:1 ratio at P = 5 mTorr. MZO deposition was done without intentional substrate heating. A more detailed description of the MZO deposition process and deposition parameters may also be found in the literature [22]. Kelvin probe (KP Technology) was utilized to measure the work function of MZO, and absolute value were obtained by normalizing with respect to a gold film standard measured concurrently. Several MZO combinatorial libraries were placed in the desiccator and work function measurements were taken periodically to track changes for roughly a 6-month period. These "aged" MZO films were then used to fabricate devices at the Colorado School of Mines (CSM). In addition, I-V measurements were done on as-deposited MZO films for carrier concentration calculations. Optical transmission measurements for MZO thin films were performed using Cary UV-Vis spectrophotometer. Tauc plots were then constructed based on UV-Vis transmission data to determine the direct band gap of MZO thin films.

To evaluate the transferability and robustness of the MZO deposition process, combinatorial MZO libraries prepared at CSM were turned into CdTe-based devices at three different research facilities: CSM, the National Renewable Energy Laboratory (NREL), and Colorado State University (CSU). For CSM devices, 3.5 μm CdTe was deposited on top of TEC10/MZO substrates using vapor transport deposition with substrate

held at 420 °C. Nitrogen was used as a carrier gas at 375 sccm while oxygen was supplied in the background at 38 sccm. CdCl₂ treatment was performed in a tube furnace in a 50/50 vol% nitrogen/oxygen ambient. CdCl₂-treated samples were soaked for 2 min in 0.1 mM CuCl₂ solution and annealed on a hot plate for 30 min at 170–180 $^{\circ}$ C. Au contacts were thermally evaporated through a physical mask on top of CuCl2-treated samples. Devices with an area of 0.079 cm² were manually scribed with a blade and indium was soldered on the edges of the TEC substrate as a front contact. Devices fabricated at NREL consisted of 4 μm CdTe deposited by close space sublimation (CSS), CdCl2 treatment at 430 °C for 10 min in 320/80 sccm He/O2. CuCl2 treatment, and Au contact. Devices prepared at CSU consisted of 4 µm CdTe deposited by CSS, CdCl₂ treatment at 400-450 °C, CuCl doping followed by Te evaporation and the back contact consisting of C/Ni paste. The detailed descriptions of device fabrication at NREL [15] and CSU [23] are available in the literature. An important distinction is that oxygen was present in the ambient used for both CdTe deposition and CdCl2 activation at both NREL and CSM, while the CSU process was nominally oxygen-free. NREL CdCl₂ activation was performed at 430 °C.

Time of flight secondary ion mass spectroscopy (TOF-SIMS) was employed to study the MZO films both as-deposited and in completed devices. Access to the MZO in the latter case was provided using a thermomechanical liftoff approach which results in cleavage at the MZO-CdTe interface [24]. Composition-depth profiling was performed using 500 eV $\rm O^{2+}$ ions. Transmission Electron Microscopy (TEM) was used to investigate the structure of the CdTe films. TEM samples were prepared by focused ion beam (FIB) milling using a dual beam FEI Nova 600 nanolab. A standard in situ lift out method described previously was employed for sample preparation [25]. Device performance was evaluated using a solar simulator at light intensity of 1-sun.

3. Results and discussion

3.1. Optimization of device performance

3.1.1. MZO thickness

Fig. 1 shows J-V curves of CdTe devices fabricated with MZO thickness variation of 25–200 nm, and optimal MZO band gap of $\sim\!3.5$ eV [22] identified in our recent work for the CSM CdTe device process with CdCl $_2$ treatment done at 430 °C for 30 min. Similarly to what was reported in literature [10], the efficiency improves as the MZO film thickness increases from 25 to 100 nm, then stays relatively unchanged in the 100–200 nm thickness range. The improvement in performance is mainly due to FF and $V_{\rm oc}$. Higher concentration of defects at the CdTe/MZO interface could be the reason for the lower performance of

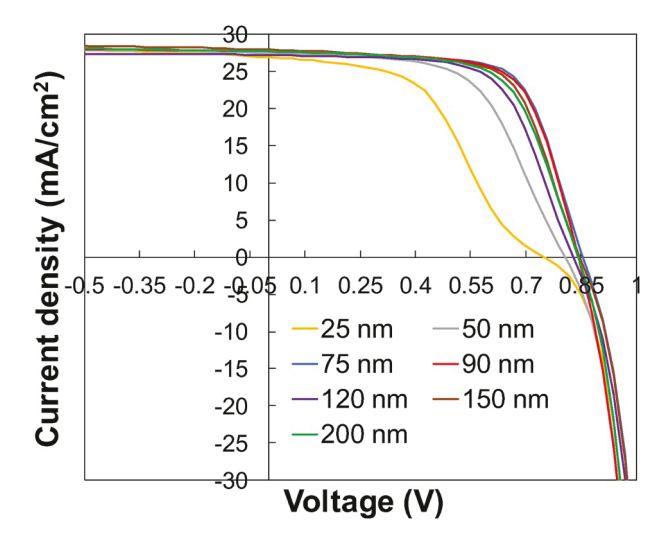


Fig. 1. J-V curves for MZO thickness range of 25-200 nm.

the thin MZO films (<50 nm) [11,16] as films are grown on the rough FTO substrate [15]. Significant drop in V_{oc} and FF for devices with 25 nm MZO film are consistent with modeled performance of devices when a higher concentration of acceptor-like defects is present at the MZO/CdTe interface [16]. It is somewhat surprising that even the thickest 200 nm film produced relatively high FFs, considering that MZO films are fully insulating and were unmeasurable with a standard colinear 4 point probe. Based on this thickness study, MZO films with thickness of 80–120 nm were used for further optimization.

3.1.2. CdCl₂ temperature

One of the advantages of MZO over CdS is that it allows for higher temperatures to be used during the CdCl₂ treatment. In the past at CSM devices employing CdS window layer experienced delamination for CdCl₂ treatments at temperatures >405 °C. Performing CdCl₂ treatment at elevated temperature should produce larger CdTe grains [26,27], which in turn would help minimize the effects of grain boundary recombination [5] and improve FF. Fig. 2 below illustrates J-V parameters versus CdCl₂ treatment temperature and time. For a 10-min treatment, the efficiency is optimized at $T=440\,^{\circ}C$. The improvement in efficiency is mainly due to improvement in V_{oc}. On the other hand, the drop in efficiency with greater activation temperatures is due to both V_{oc} and FF deterioration. While devices with >16% efficiency were obtained at T = 440 $^{\circ}$ C, there was evidence of rollover in the J-V curves suggesting that this temperature was too aggressive. As shown in Fig. 2 it was found that similar or somewhat improved performance was achieved by reducing the temperature to 430 °C and extending the treatment time to 30 min. From visual inspection of the device stack no evidence of delamination was observed for temperatures up to 450 °C, while sample treated at 460 °C had spots that appeared hazy white in color, indicating the presence of some delamination at the front of the device stack.

Cross-sectional TEM was employed to better understand the observed efficiency of the devices. Fig. 3 shows cross-sectional TEM images of the device stack from samples without $CdCl_2$ activation, under optimal conditions ($T=430~^{\circ}C/30~\text{min}$), and with excessive treatment ($T=450~^{\circ}C/10~\text{min}$). CdS baseline device with $CdCl_2$ treatment performed at $400~^{\circ}C$ is also shown for comparison. As can be seen from the images, as-deposited CdTe grains are small ($<1~\mu m$) with significant numbers of defects and dislocations, with further deterioration approaching the MZO/CdTe interface. Very similar morphology was reported in literature [28] for an as-deposited sample without $CdCl_2$

treatment. It is well known that the $CdCl_2$ treatment results in grain growth, recrystallization and grain boundary passivation in CdTe absorbers [26]. Devices that underwent $CdCl_2$ treatment display large, equi-axed grains several microns in size that provide pathways uninterrupted by grain boundaries from the front to the back contact. However, when the treatment exceeds critical conditions the grains appear to separate from one another, which is evident from the dark regions at the grain boundaries, indicating development of voids in-between grains. This grain separation is consistent with what has been reported in literature [28], although temperatures above 450 °C were required to see this effect.

3.1.3. Optimized devices

Fig. 4 illustrates the J-V curves of devices with optimized thickness of MZO ($\sim\!100$ nm) and optimized CdCl $_2$ treatment at different MZO band gaps, extracted from Tauc plots. From the figure we see that the J-V curves follow the trends that were previously described in the literature [10]. Flat or slight "spike" conduction band alignment at the front is desirable. When the band gap is too high, the conduction band of MZO is positioned higher than that of CdTe, causing a large barrier at the interface. This primarily results in loss of FF and some drop in J_{sc} . On the contrary, when the band gap is too low and the conduction band position of MZO is lower than CdTe and a so-called "cliff" is formed, causing recombination at the front interface and leading to loss of V_{oc} .

Optimal MZO band gap of ~3.5 eV results in efficiency of almost 16%. It is important to note that these devices were produced with significant amounts of oxygen present both in the CdTe growth and CdCl₂ treatment ambients, as described in the Materials and Methods section. Several research groups have reported significantly reduced performance (<10% efficient) when oxygen was present during processing [15,16,29]. It was hypothesized, based on simulations and device results, that removal of oxygen from the CdCl2 treatment atmosphere is necessary to keep the oxygen vacancy concentration of the MZO layer high enough (>10¹⁶ cm⁻³) to allow band bending and tunneling to reduce recombination at the junction [16]. Recently, increased front contact barrier height was measured using admittance spectroscopy, when the CdCl₂ treatment was performed in an oxygen containing atmosphere [30]. Although important, the band bending due to emitter doping and barrier height alone do not seem to provide full explanation for the lower performance of devices employing conventional MZO when oxygen is present in device processing ambient

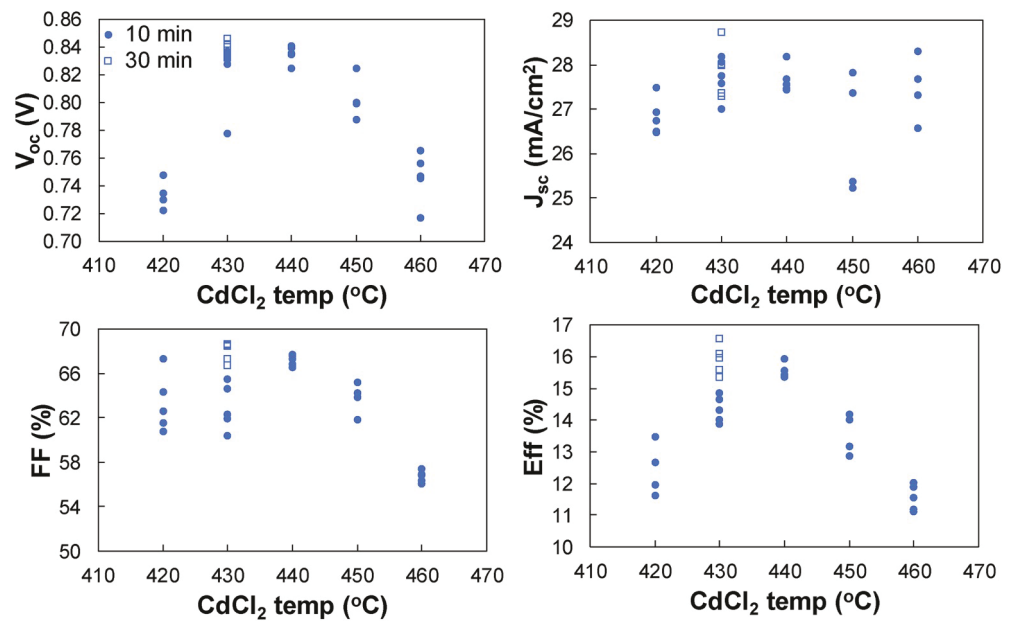


Fig. 2. J-V parameters of devices as a function of CdCl₂ activation temperature for treatment times of 10 (full circles) and 30 (open squares) minutes.

Fig. 3. Cross-sectional TEM images of CdTe solar cells: a) no CdCl₂ treatment, b) CdCl₂-treated at 400 °C with CdS window, c) CdCl₂-treated at 430 °C with MZO window, and d) CdCl₂-treated at 450 °C with MZO window.

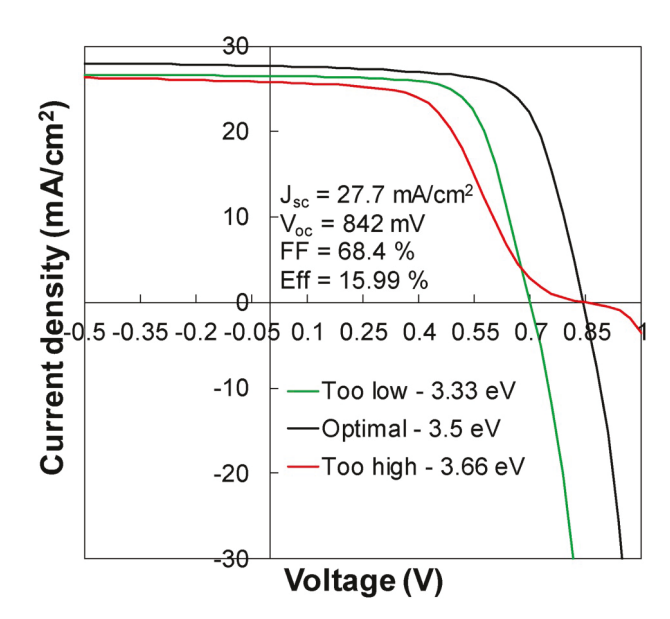


Fig. 4. J-V curves of optimized CSM devices at too low, optimal, and too high MZO band gaps with oxygen being present in both the CdTe growth and $CdCl_2$ treatment ambients.

because poor performance with S-kink in J-V curves was observed even for MZO band gap of <3.5 eV, which typically results in flat or slightly positive conduction band offset at the MZO/CdTe interface [15]. Recent modeling indicated that the formation of S-kink in this case could be explained by higher density of acceptor-like defects at the MZO/CdTe interface [16]. Good device performance achieved here seems to suggest that reactively sputtered MZO is more stable during device processing both with and without oxygen and more details will be provided in the subsequent sub-sections. From Fig. 4 it is apparent that even for the optimal device FF and Voc both have room for improvement. We hypothesize that the biggest additional gain in devices using optimal MZO is through optimization of the back contact, especially the recipe for rapid thermal processing (RTP) of ZnTe:Cu, and this work is ongoing [31,32]. Copper has a significant effect on recrystallization and interdiffusion at the back of the device stack so careful tailoring of back contact activation is very important for optimized performance [33]. As shown above MZO devices have large CdTe grains, which are bigger than CdTe grains in devices with CdS window layer. As such it would most likely require a different RTP sequence and temperatures to balance bulk and grain boundary Cu diffusion in CdTe.

3.1.4. Transferability

To study robustness and transferability, MZO films prepared by reactive co-sputtering were converted into CdTe devices at both NREL and CSU, and the results were compared to CdTe devices fabricated at CSM. Fig. 5 shows J-V curves at 3 representative band gaps (too low/optimal/too high) from combinatorial FTO/MZO superstrates prepared at CSM and converted into devices at NREL and CSU, respectively. Note

that both institutions employed their standard process sequences without further optimization. Both sets displayed good rectification at the optimal MZO composition and either reduced V_{oc} or diminished FF when the Mg level is insufficient or in excess, respectively. These trends were consistent with literature [10] and the CSM devices in Fig. 4. An efficiency of 15.5% was achieved for NREL devices and the optimal MZO band gap was \sim 3.5 eV. The V_{oc} of 810 mV is lower than that of optimal CSM device at 843 mV, again indicating that the Cu doping can be further optimized for higher efficiency. Devices fabricated at CSU reached an efficiency of 16.6% at an MZO band gap of \sim 3.6 eV. There is a slight difference of 0.1 eV in optimal MZO band gaps which may reflect the fact that CSM and NREL devices had oxygen in the processing ambient while CSU devices were made in an oxygen-free environment. In particular, the FF of the CSU devices were significantly improved, which may reflect the absence of oxygen and/or a different back contact scheme. Thus, while the reactively sputtered films were much more resilient to the presence of oxygen, best performance may require its omission.

In order to study the stability of our MZO films during processing we used TOF-SIMS to compare Zn and Mg concentrations in an as-deposited film with that from a delaminated device. Fig. 6 below shows depth profiles (Mg, Zn, Sn) through the MZO layer and into the underlying FTO. The bulk Mg and Zn counts are identical in both films. In the processed device, both the Mg and Zn counts are initially low near the surface, but their ratio in this region is nominally identical to the asdeposited device. This artifact is attributed to imperfect delamination which leads to roughness and there was residual CdTe present. It is wellknown that CdS undergoes significant interdiffusion and alloying with CdTe during device processing [34,35]. If significant interdiffusion with CdTe had occurred one would expect changes in the MZO composition due to cation (Mg-Zn/Cd) and/or anion (O-Te) exchange. The nominally identical Zn and Mg counts across the bulk of the as-deposited and processed film suggest that if CdTe/MZO interdiffusion occurs during processing it is minimal on the MZO side, and its extent does not exceed the level of interfacial roughness. Depth profile data also suggests that MZO/FTO interdiffusion during processing is negligible. The Mg/Zn profiles into the FTO are nominally identical for as-deposited and processed films. The slopes of the Sn profiles near the MZO/FTO interface are likewise similar, with a slight tail forming in a processed film which is most likely an artifact associated with delamination. Recently published results [15] suggested that the composition of the MZO may be changing during device processing. The published XPS measurements showed that the Mg concentration in MZO from a "peeled" device as well as pre-heated film decreased compared to the as-deposited MZO, indicating preferential loss of Mg during processing. The TOF-SIMS depth profile data presented in Fig. 6 further points to the stability and process resilience of reactively sputtered MZO films.

3.2. Stability of reactively sputtered MZO

3.2.1. Kelvin probe

To study the stability of the MZO films, several combinatorial samples were placed in a desiccator and Kelvin probe measurements were performed periodically for about 6 months. Kelvin probe measures the

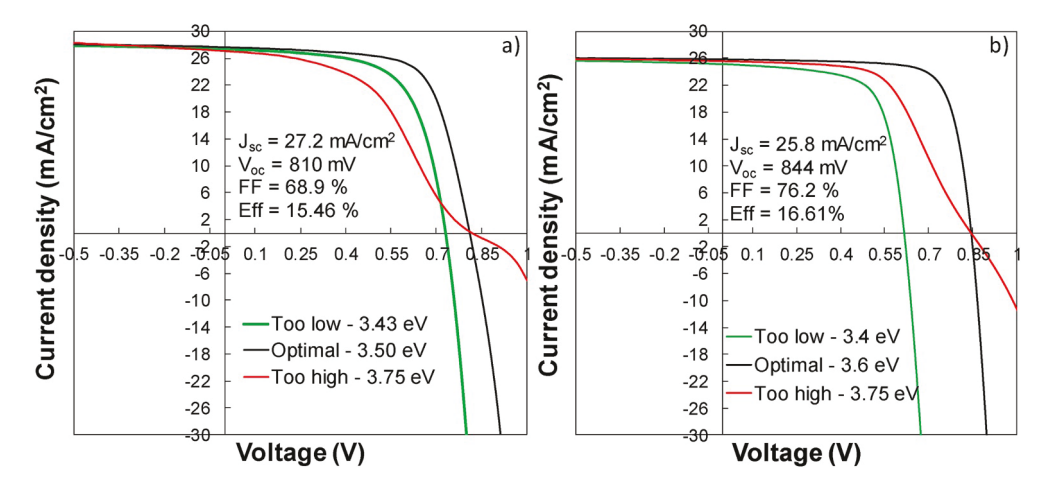


Fig. 5. J-V curves of devices with too low, optimal, and too high MZO band gaps across combinatorial MZO samples employing a) NREL's CdTe and CdCl₂ processes; b) CSU's device processing.

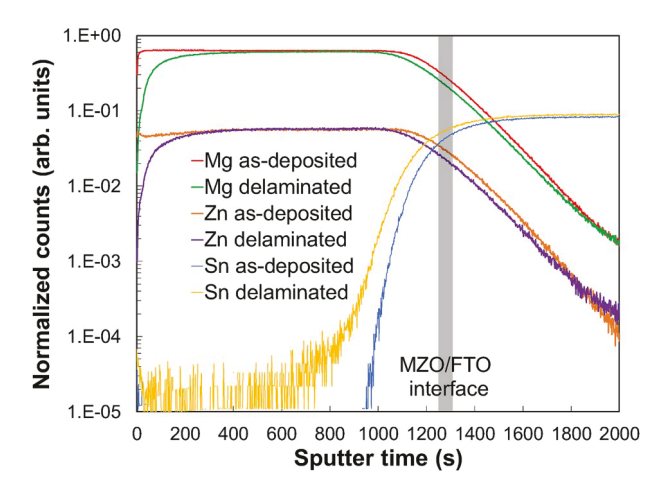


Fig. 6. Normalized Zn and Mg secondary ion counts from TOF-SIMS depth profile of optimal band gap MZO in as-deposited form and then from a delaminated device.

work function and is a highly surface sensitive technique. Therefore, monitoring the work function of a MZO film could potentially be used to track any changes that occur on the surface [14,22]. Fig. 7 below illustrates work function variation across one of the combinatorial samples. The MZO band gap is plotted on the secondary axis. The initial measurement shows significant variation of the work function across a 3-inch substrate. The decrease in work function reflects the increasing band gap (increasing Mg concentration). This is consistent with the "common anion" rule [36], which states that the valence band energy of the ternary alloy is nominally fixed and changes in the band gap are due primarily to the movement of the conduction band. Furthermore, assuming that the doping of the MZO stays relatively unchanged, addition of Mg to ZnO would cause an upward shift in the position of the Fermi level, which means the work function would decrease. It can be seen from the figure that the gradient in the work function remains for the duration of the "aging" test. Although there is some variation in the absolute values of the work function there are no systematic changes with time, and the qualitative trends are similar. These results suggest that there is no significant change to the surface of the MZO film during the testing period.

Fig. 8a shows a schematic energy level diagram for MZO. Using the work function (ϕ) measurements the position of the Fermi level and approximate carrier concentration in the MZO films may be estimated as described below. Equations (1)–(3) below describe the relationship

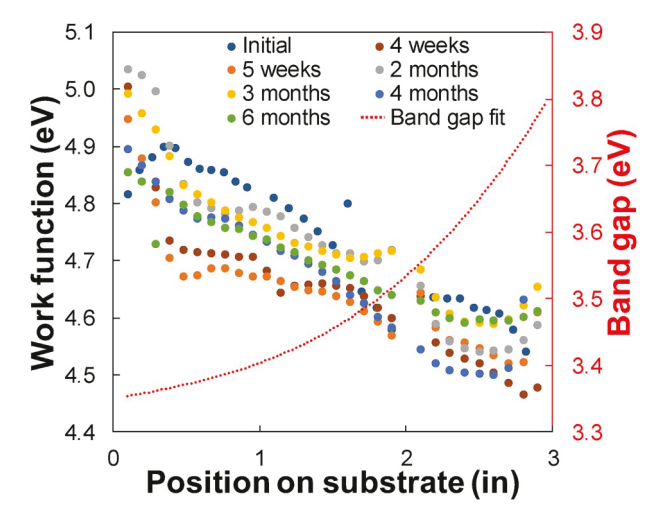


Fig. 7. Work function measurements performed over the course of 6 months using Kelvin probe across a 3 inch combinatorial MZO sample. Sample was stored in an atmospheric pressure desiccator in-between measurements.

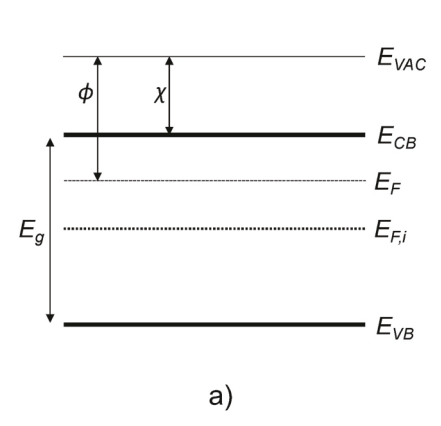
between carrier concentration and the position of the Fermi level:

$$E_F - E_{F,i} = kT \ln \left(\frac{n}{n_i}\right) \tag{1}$$

$$n_i = \exp\left(\frac{E_g}{2kT}\right)\sqrt{N_C N_V} \tag{2}$$

$$E_{F,i} = \frac{E_C + E_V}{2} + \frac{kT}{2} \ln \left(\frac{N_V}{N_C} \right)$$
 (3)

where $E_{F,i}$ is intrinsic Fermi level position, E_F is the actual Fermi level position, n_i is intrinsic carrier concentration, n_i is carrier (electron) concentration, E_g is the band gap of the material, E_C is the conduction band position, E_V is the valence band position, E_V is the Boltzmann constant, E_V is the valence band position, E_V is the Boltzmann constant, E_V is the valence band E_V are density of states in conduction and valence bands, respectively. The band gap of pure reactively sputtered ZnO is 3.26 eV. If we assume E_V 1.8E+19 cm³, E_V 1.8E+18 cm³ [37], we can calculate the intrinsic carrier concentration and the actual carrier (electron) concentration required to shift the position of the Fermi level closer to the conduction band at E_V 1.8E+19 cm³, E_V 1.9C 2.8E+18 cm³ [37], we use an electron affinity of 4.5 eV for ZnO and assume that increases in band gap



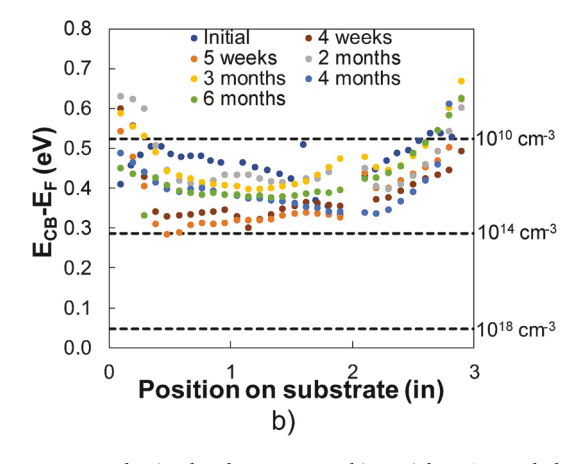


Fig. 8. a) Energy level diagram for MZO; b) estimated Fermi level with respect to conduction band across a combinatorial MZO sample based on work function measurements. Dashed lines indicate the calculated positions of the Fermi level with respect to conduction band when carrier concentration is at 10^{10} , 10^{14} or 10^{18} cm³.

with the addition of Mg reflect only changes in its conduction band position, or an equivalent decrease in χ . The position of the Fermi level with respect to the conduction band is simply the difference between the work function measured by Kelvin probe and the electron affinity of MZO derived from its band gap. The carrier concentration is then calculated using Equation (1), and these assumptions mean that the resulting estimates of carrier concentrations presented below represent an upper bound of their value.

Fig. 8b below illustrates the calculated position of the Fermi level with respect to conduction band of a combinatorial MZO sample based on work function measurements displayed in Fig. 7. Dashed lines in Fig. 8b indicate theoretical positions of the Fermi level when carrier concentration in MZO is 10^{10} , 10^{14} or 10^{18} cm⁻³. Across most of the MZO library the position of the Fermi level is 0.3-0.5 eV below the conduction band which corresponds to carrier concentrations in the 10^{10} - 10^{14} cm⁻³ range. Note that this variability reflects the small day to day fluctuations in the measured work function, but for any given measurement the carrier concentration is essentially constant across the MZO library. To independently validate carrier concentration values, simple resistors were fabricated by depositing Al contacts onto FTO/ MZO substrates. The resulting values of resistivity were in the 10⁶ Ohm*cm range, which corresponds to carrier concentrations on the order of $10^{11} \, \mathrm{cm}^{-3}$, assuming mobility of $20 \, \mathrm{cm}^2 / \mathrm{V*s}$. Though debate in literature remains, native point defects are usually considered to control conductivity in ZnO films [40,41]. The data in Fig. 8 and the carrier concentrations calculated from I-V measurements seem to point to the fact that as-deposited MZO films have stable (equilibrium) concentration of point defects that leads to films being insulating and makes them relatively insensitive to the presence of oxygen in high temperature processing steps. We also note that these MZO film remained insulating even after vacuum annealing at device processing temperatures. An ideal emitter should have carrier concentrations $\sim 10^{18}$ cm⁻³ [12], and this remains an unresolved challenge with MZO due to the amphoteric nature of Mg [42]. The reactive sputtering approach described here may be applied to host of compounds, and the combinatorial approach may be very useful in rapidly evaluating new alloys for this application.

3.2.2. Aged vs. fresh devices

Lastly, MZO films devices were fabricated from the "aged" combinatorial sample. Fig. 9 compares of J-V curves of CdTe devices made at CSM on fresh vs. aged MZO at equivalent band gaps. It is evident from the data that the device performance is not affected significantly with storing of MZO in the desiccator for a period of 6 months, which has not been the case generally for MZO grown from fixed composition oxide targets. In both cases efficiencies of around 14% are achieved—the differences are within the noise of our standard device process. Neither

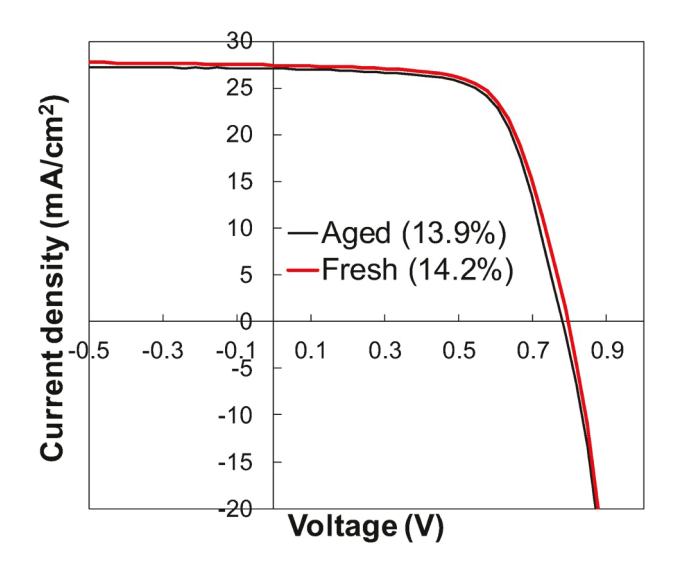


Fig. 9. Comparison of J-V curves of devices from a "fresh" and "aged" combinatorial sample.

fresh nor aged MZO surfaces were cleaned prior to device fabrication. This is important to note because static TOF-SIMS measurements indicated significant increase in both carbon and hydrogen counts for the surface of aged MZO film, pointing to the accumulation of hydrocarbons on the surface. These hydrocarbons could potentially have some negative effects on performance, but it doesn't seem to be detrimental based on the data in Fig. 9.

4. Conclusions

Reactive co-sputtering was shown to produce robust, high quality MZO films, and the formation of combinatorial libraries accelerated identification of optimal MZO composition. High efficiency (\sim 16%) CdTe devices were produced across multiple device platforms, with and without the presence of oxygen in device processing steps. The reactively sputtered MZO films were shown to be stable with respect to time and through high temperature CdTe device fabrication. The resilience and stability of MZO were attributed to stable (equilibrium) concentration of point defects in the as-deposited films, which was consistent with work function measurements over the period of 6 months. The combinatorial approach described here is expected to be useful for identifying both the optimal MZO composition to match ternary absorbers (i.e. CdSe $_{\rm V}$ Te $_{\rm I-V}$), and for discovery of other improved emitter

alternatives beyond MZO.

Declaration of competing interest

The authors declare that they have no known competing financial interests or personal relationships that could have appeared to influence the work reported in this paper.

CRediT authorship contribution statement

Yegor Samoilenko: Conceptualization, Methodology, Investigation, Formal analysis, Writing - original draft, Writing - review & editing. Gavin Yeung: Methodology, Investigation, Writing - review & editing. Amit H. Munshi: Investigation, Writing - review & editing. Ali Abbas: Investigation, Writing - review & editing. Carey L. Reich: Investigation, Writing - review & editing. Michael Walker: Investigation, Writing - review & editing. Matthew O. Reese: Investigation, Writing - review & editing. Andriy Zakutayev: Investigation, Writing - review & editing. J. Michael Walls: Supervision, Writing - review & editing. Walajabad S. Sampath: Supervision, Writing - review & editing. Colin A. Wolden: Conceptualization, Supervision, Project administration, Writing - review & editing.

Acknowledgements

The CSM authors are grateful to the National Science Foundation (NSF) through award number CBET-1706149. We would also like to thank Deborah McGott for providing training on CdTe processing at NREL. The use of the TOF-SIMS system at CSM was supported by the NSF under Grant No.1726898. The Loughborough authors would like to thank support from the EPSRC for funding this research through project EP/N026438/1. Authors at CSU would like to acknowledge support from NSF AIR, NSF I/UCRC and US DOE PVRD programs. Work at CSU was supported by NSF award 1540007, NSF AIR-RA program 1538733 and US Department of Energy SIPS award DE-EE0008177. The CdTe work at NREL was supported by the U.S. Department of Energy under Contract No. DE-AC36-08GO28308 with Alliance for Sustainable Energy, LLC, the Manager and Operator of NREL. Funding provided by the U.S. Department of Energy's Office of Energy Efficiency and Renewable Energy, Solar Energy Technology Office. Kelvin Probe measurement work at NREL was supported by U.S. Department of Energy, Office of Energy Efficiency and Renewable Energy, Fuel Cell Technologies Program, as a part of HydroGEN Energy Materials Network, under Award No. DEAC36- 08GO28308, with Alliance for Sustainable Energy, LLC, the Manager and Operator of the National Renewable Energy Laboratory. The U.S. Government retains and the publisher, by accepting the article for publication, acknowledges that the U.S. Government retains a nonexclusive, paid-up, irrevocable, worldwide license to publish or reproduce the published form of this work, or allow others to do so, for U.S. Government purposes. The views expressed in the article do not necessarily represent the views of the DOE or the U.S. Government.

Appendix A. Supplementary data

Supplementary data to this article can be found online at https://doi.org/10.1016/j.solmat.2020.110521.

References

- On 20th Anniversary, First Solar Sets 25GW Milestone for Cleaner, Thin Film Solar, First Solar, 2019.
- [2] NREL Best Research-Cell Efficiencies. https://www.nrel.gov/pv/assets/pdfs/best-research-cell-efficiencies.20190923.pdf. (Accessed 8 October 2019).
- [3] A.H. Munshi, J. Kephart, A. Abbas, J. Raguse, J.N. Beaudry, K. Barth, J. Sites, J. Walls, W. Sampath, Polycrystalline CdSeTe/CdTe absorber cells with 28 mA/ cm2 short-circuit current, IEEE J. Photovoltanics 8 (1) (2018) 310–314, https://doi.org/10.1109/jphotov.2017.2775139.

- [4] A.H. Munshi, J.M. Kephart, A. Abbas, T.M. Shimpi, K.L. Barth, J.M. Walls, W. S. Sampath, Polycrystalline CdTe photovoltaics with efficiency over 18% through improved absorber passivation and current collection, Sol. Energy Mater. Sol. Cell. 176 (2018) 9–18, https://doi.org/10.1016/j.solmat.2017.11.031.
- [5] A. Kanevce, M.O. Reese, T.M. Barnes, S.A. Jensen, W.K. Metzger, The roles of carrier concentration and interface, bulk, and grain-boundary recombination for 25% efficient CdTe solar cells, J. Appl. Phys. 121 (21) (2017) 214506, https://do. org/10.1063/1.4984320.
- [6] J.M. Burst, J.N. Duenow, D.S. Albin, E. Colegrove, M.O. Reese, J.A. Aguiar, C. S. Jiang, M.K. Patel, M.M. Al-Jassim, D. Kuciauskas, S. Swain, T. Ablekim, K. G. Lynn, W.K. Metzger, CdTe solar cells with open-circuit voltage breaking the 1 V barrier, Nat. Energy 1 (3) (2016) 16015, https://doi.org/10.1038/nenergy.2016.15.
- [7] W.K. Metzger, S. Grover, D. Lu, E. Colegrove, J. Moseley, C.L. Perkins, X. Li, R. Mallick, W. Zhang, R. Malik, J. Kephart, C.S. Jiang, D. Kuciauskas, D.S. Albin, M. M. Al-Jassim, G. Xiong, M. Gloeckler, Exceeding 20% efficiency with in situ group V doping in polycrystalline CdTe solar cells, Nat. Energy 4 (10) (2019) 837–845, https://doi.org/10.1038/s41560-019-0446-7.
- [8] T.A.M. Fiducia, B.G. Mendis, K. Li, C.R.M. Grovenor, A.H. Munshi, K. Barth, W. S. Sampath, L.D. Wright, A. Abbas, J.W. Bowers, J.M. Walls, Understanding the role of selenium in defect passivation for highly efficient selenium-alloyed cadmium telluride solar cells, Nat. Energy 4 (6) (2019/06/01 2019) 504–511, https://doi.org/10.1038/s41560-019-0389-z.
- [9] X. Zheng, D. Kuciauskas, J. Moseley, E. Colegrove, D.S. Albin, H. Moutinho, J. N. Duenow, T. Ablekim, S.P. Harvey, A. Ferguson, W.K. Metzger, Recombination and bandgap engineering in CdSeTe/CdTe solar cells, Apl. Mater. 7 (7) (2019), 071112, https://doi.org/10.1063/1.5098459.
- [10] J.M. Kephart, J.W. McCamy, Z. Ma, A. Ganjoo, F.M. Alamgir, W.S. Sampath, Band alignment of front contact layers for high-efficiency CdTe solar cells, Sol. Energy Mater. Sol. Cell. 157 (2016) 266–275, https://doi.org/10.1016/j. solmat.2016.05.050, 2016/12/01/2016.
- [11] T. Song, A. Kanevce, J.R. Sites, Emitter/absorber interface of CdTe solar cells, J. Appl. Phys. 119 (23) (2016) 233104, https://doi.org/10.1063/1.4953820.
- [12] T. Ablekim, E. Colegrove, W.K. Metzger, Interface engineering for 25% CdTe solar cells, ACS Appl. Energy Mater. (2018), https://doi.org/10.1021/acsaem.8b01173.
- [13] J.M. Kephart, A. Kindvall, D. Williams, D. Kuciauskas, P. Dippo, A. Munshi, W. S. Sampath, Sputter-deposited oxides for interface passivation of CdTe photovoltaics, IEEE J. Photovoltanics 8 (2) (2018) 587–593, https://doi.org/10.1109/jphotov.2017.2787021.
- [14] F. Bittau, S. Jagdale, C. Potamialis, J.W. Bowers, J.M. Walls, A.H. Munshi, K. L. Barth, W.S. Sampath, Degradation of Mg-doped zinc oxide buffer layers in thin film CdTe solar cells, Thin Solid Films (2019) 137556, https://doi.org/10.1016/j.tsf.2019.137556.
- [15] T. Ablekim, C. Perkins, X. Zheng, C. Reich, D. Swanson, E. Colegrove, J. Duenow, D. Albin, S. Nanayakkara, M.O. Reese, T. Shimpi, W. Sampath, W.K. Metzger, Tailoring MgZnO/Cd(Se)Te interfaces for photovoltaics, IEEE J. Photovoltanics 9 (3) (2019) 888–892, https://doi.org/10.1109/JPHOTOV.2018.2877982.
- [16] D.-B. Li, Z. Song, R.A. Awni, S.S. Bista, N. Shrestha, C.R. Grice, L. Chen, G. K. Liyanage, M.A. Razooqi, A.B. Phillips, M.J. Heben, R.J. Ellingson, Y. Yan, Eliminating S-kink to maximize the performance of MgZnO/CdTe solar cells, ACS Appl. Energy Mater. 2 (4) (2019) 2896–2903, https://doi.org/10.1021/2022889 050033
- [17] S. Ren, H. Wang, Y. Li, H. Li, R. He, L. Wu, W. Li, J. Zhang, W. Wang, L. Feng, Rapid thermal annealing on ZnMgO window layer for improved performance of CdTe solar cells, Sol. Energy Mater. Sol. Cell. 187 (2018) 97–103, https://doi.org/10.1016/j.solmat.2018.06.033, 2018/12/01/2018.
- [18] S. Han, D.Z. Shen, J.Y. Zhang, Y.M. Zhao, D.Y. Jiang, Z.G. Ju, D.X. Zhao, B. Yao, Characteristics of cubic MgZnO thin films grown by radio frequency reaction magnetron co-sputtering, J. Alloys Compd. 485 (1–2) (2009) 794–797, https://doi. org/10.1016/j.jallcom.2009.06.088.
- [19] Y. Matsumoto, M. Murakami, Z. Jin, A. Ohtomo, M. Lippmaa, M. Kawasaki, H. Koinuma, Combinatorial laser molecular beam epitaxy (MBE) growth of Mg-Zn-O alloy for band gap engineering, Jpn. J. Appl. Phys. 38 (1999) L603–L605.
- [20] A. Mavlonov, S. Richter, H. von Wenckstern, R. Schmidt-Grund, J. Lenzner, M. Lorenz, M. Grundmann, Doping efficiency and limits in (Mg,Zn)O:Al,Ga thin films with two-dimensional lateral composition spread, Phys. Status Solidi 212 (12) (2015) 2850–2855, https://doi.org/10.1002/pssa.201431932.
- [21] P.P. Rajbhandari, A. Bikowski, J.D. Perkins, T.P. Dhakal, A. Zakutayev, Combinatorial sputtering of Ga-doped (Zn,Mg)O for contact applications in solar cells, Sol. Energy Mater. Sol. Cell. 159 (2017) 219–226, https://doi.org/10.1016/j. solmat.2016.09.003, 1//2017.
- [22] Y. Samoilenko, G. Yeung, A. Zakutayev, M.O. Reese, C.A. Wolden, Combinatorial study of MZO emitters for CdTe-based solar cells, in: Proc. IEEE PVSC, 46, 2019, pp. 2498–2502, https://doi.org/10.1109/PVSC40753.2019.8980695.
- [23] D.E. Swanson, J.M. Kephart, P.S. Kobyakov, K. Walters, K.C. Cameron, K.L. Barth, W.S. Sampath, J. Drayton, J.R. Sites, Single vacuum chamber with multiple close space sublimation sources to fabricate CdTe solar cells, J. Vac. Sci. Technol.: Vac. Surf. Film 34 (2) (2016), 021202, https://doi.org/10.1116/1.4941071.
- [24] D.L. McGott, M.D. Kempe, S. Glynn, N. Bosco, T.M. Barnes, N.M. Haegel, C. A. Wolden, M.O. Reese, Thermomechanical lift-off and recontacting of CdTe solar cells, ACS Appl. Mater. Interfaces 10 (51) (Dec 26 2018) 44854–44861, https://doi.org/10.1021/acsami.8b16476.
- [25] A. Abbas, G.D. West, J.M. Bowers, P. Isherwood, P.M. Kaminski, B. Maniscalco, P. Rowley, J.M. Walls, K. Barricklow, W.S. Sampath, K.L. Barth, The effect of cadmium chloride treatment on close-spaced sublimated cadmium telluride thin-

- film solar cells, IEEE J. Photovoltanics 3 (4) (2016) 1361–1366, https://doi.org/10.1109/JPHOTOV.2013.2264995.
- [26] H.R. Moutinho, M.M. Al-Jassim, D.H. Levi, P.C. Dippo, L.L. Kazmerski, Effects of CdCl2 treatment on the recrystallization and electro-optical properties of CdTe thin films, J. Vac. Sci. Technol.: Vac. Surf. Film 16 (3) (1998) 1251, https://doi.org/ 10.1116/1.581269.
- [27] M. Amarasinghe, E. Colegrove, H. Moutinho, D. Albin, J. Duenow, S. Johnston, J. Kephart, W. Sampath, M. Al-Jassim, S. Sivananthan, W.K. Metzger, Influence of CdTe deposition temperature and window thickness on CdTe grain size and lifetime after CdCl 2 recrystallization, IEEE J. Photovoltanics 8 (2) (2018) 600–603, https://doi.org/10.1109/jphotov.2018.2790701.
- [28] M. Amarasinghe, E. Colegrove, J. Moseley, H. Moutinho, D. Albin, J. Duenow, S. Jensen, J. Kephart, W. Sampath, S. Sivananthan, M. Al-Jassim, W.K. Metzger, Obtaining large columnar CdTe grains and long lifetime on nanocrystalline CdSe, MgZnO, or CdS layers, Adv. Energy Mater. 8 (11) (2018) 1702666, https://doi.org/ 10.1002/aenm.201702666.
- [29] A.E. Delahoy, S. Peng, P. Patra, S. Manda, A. Saraf, Y. Chen, X. Tan, K.K. Chin, Cadmium tin oxide and zinc magnesium oxide prepared by hollow cathode sputtering for CdTe photovoltaics, MSR Adv. 2 (2017) 3203–3214.
- [30] R.A. Awni, D.-B. Li, Z. Song, S.S. Bista, M.A. Razooqi, C.R. Grice, L. Chen, G. K. Liyanage, C. Li, A.B. Phillips, M.J. Heben, R.J. Ellingson, J.V. Li, Y. Yan, Influences of buffer material and fabrication atmosphere on the electrical properties of CdTe solar cells, Prog. Photovoltaics Res. Appl. (2019), https://doi.org/10.1002/pip.3192.
- [31] J. Li, D.R. Diercks, T.R. Ohno, C.W. Warren, M.C. Lonergan, J.D. Beach, C. A. Wolden, Controlled activation of ZnTe:Cu contacted CdTe solar cells using rapid thermal processing, Sol. Energy Mater. Sol. Cell. 133 (2015) 208–215, https://doi.org/10.1016/j.solmat.2014.10.045.
- [32] C.A. Wolden, A. Abbas, J. Li, D.R. Diercks, D.M. Meysing, T.R. Ohno, J.D. Beach, T. M. Barnes, J.M. Walls, The roles of ZnTe buffer layers on CdTe solar cell

- performance, Sol. Energy Mater. Sol. Cell. 147 (4//2016) 203–210, https://doi.org/10.1016/j.solmat.2015.12.019.
- [33] Y. Samoilenko, A. Abbas, J. Michael Walls, C.A. Wolden, Copper-induced recrystallization and interdiffusion of CdTe/ZnTe thin films, J. Vac. Sci. Technol.: Vac. Surf. Film 36 (3) (2018), 031201, https://doi.org/10.1116/1.5023501.
- [34] B.E. McCandless, L.V. Moulton, R.W. Birkmire, Recrystallization and sulfur diffusion in CdCl2-treated CdTe/CdS thin films, Prog. Photovoltaics Res. Appl. 5 (1997) 249–260.
- [35] R.G. Dhere, D. Albin, D.H. Rose, S.E. Asher, K.M. Jones, M.M. Al-Jassim, H. R. Moutinho, P. Sheldon, Intermixing at the CdS/CdTe interface and its effect on device performance, Mater. Res. Soc. 426 (1996) 361–366.
- [36] A. Klein, Energy band alignment in chalcogenide thin film solar cells from photoelectron spectroscopy, J. Phys. Condens. Matter 27 (13) (Apr 10 2015) 134201, https://doi.org/10.1088/0953-8984/27/13/134201.
- [37] M. Gloeckler, A.L. Fahrenbruch, J.R. Sites, Numerical Modeling of CIGS and CdTe solar cells: setting the baseline, in: 3rd World Conference of Photovoltaic Energy Conversion, 2003.
- [38] K.B. Sundaram, A. Khan, Work function determination of zinc oxide films, J. Vac. Sci. Technol: Vac. Surf. Film 15 (2) (1997) 428–430, https://doi.org/10.1116/ 1.59602
- [39] L.J. Brillson, Y. Lu, ZnO Schottky barriers and Ohmic contacts, J. Appl. Phys. 109 (12) (2011) 121301, https://doi.org/10.1063/1.3581173.
- [40] L. Liu, Z. Mei, A. Tang, A. Azarov, A. Kuznetsov, Q.-K. Xue, X. Du, Oxygen vacancies: the origin of n-type conductivity in ZnO, Phys. Rev. B 93 (2016) 23, https://doi.org/10.1103/PhysRevB.93.235305.
- [41] A. Janotti, C.G. Van de Walle, Oxygen vacancies in ZnO, Appl. Phys. Lett. 87 (12) (2005) 122102, https://doi.org/10.1063/1.2053360.
- [42] O. Bierwagen, Indium oxide—a transparent, wide-band gap semiconductor for (opto)electronic applications, Semicond. Sci. Technol. 30 (2) (2015), https://doi. org/10.1088/0268-1242/30/2/024001, 024001, 2015/01/19 2015.